

EXPERIMENTAL AND NUMERICAL DRILL STRING MODELING FRICTION INDUCED STICK-SLIP

Bruno C. C. Andrade*¹, Cesar A. L. L. Fosenca¹, Hans. I. Weber¹

¹ Pontificia fUniversidade Católica do Rio de Janeiro
cayres.bruno@gmail.com
cesarlampe88@gmail.com
hans@puc-rio.br

Keywords: Torsional Vibration, Drill String Dynamics, Stick-Slip Phenomenon. Nonlinear Dynamics.

Abstract. *A successful oil and gas prospecting requires many efforts to overcome the encountered challenges, such as axial, lateral and torsional vibrations. These phenomena may cause premature component failures of the drilling system, dysfunction of measurement devices, and increase of time and costs of the prospecting process. Torsional vibrations are present in most drilling processes and may reach an undesired severity state: stick-slip. An improved understanding of the stick-slip phenomenon may provide tools to avoid the increase of prospecting time and costs, assuring the investment and success of the drilling process. In this paper, it is described a numerical/experimental procedure with a non-linear friction aiming to induce stick-slip. The friction model is based on dry friction imposed by a specially designed test rig with a braking device. The non-linear behaviour of the experimental apparatus is analysed and the numerical model will be validated comparing experimental and numerical bifurcation diagrams. Also, it is performed a sensitivity analysis of the experimental apparatus parameters.*

1 INTRODUCTION

Oil and other hydrocarbons are the primary source of global energy. However, the exploration of these hydrocarbons presents a myriad of challenges resulting mainly from lithological variation and other unanticipated natural phenomena. Among these challenges, the occurrence of vibrations generated during the drilling process is of great importance and poses several associated risks.

Due to the non-linear complexity arising from the boundary conditions, bit-rock interaction, and drill string-wellbore wall interaction the drilling system presents complex vibration phenomena. Thus, the drill strings undergo axial (longitudinal motion), lateral (whirl motion) and torsional (angular fluctuation) vibrations (see Figure 1). The damage from this undesired behaviour is worrisome, such as the premature wear of parts of the drill string and bit, downhole motors, and the interference of transmission signals measured data. This results in increased time and cost of the process. Therefore, a better understanding of these phenomena, which can occur uncoupled or coupled, is necessary.

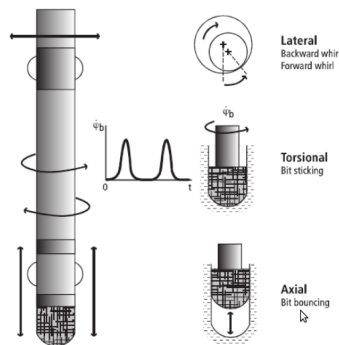


Figure 1: Types of vibration on drill string. Source: López [17].

Measurements of drill string rotation both at surface and at the bit have revealed that the drill string often behaves as a rotating torsional pendulum, i.e. the top end rotates with a constant rotary speed, whereas the bit performs a rotation with varying rotary speed consisting of a constant part and a superimposed torsional vibration [1]. In its most drastic form, the bit comes to a standstill while the top end rotates with a constant rotary speed, and then increasing the torque in the drill string until the bit suddenly comes loose again [3]: stick-slip.

In this paper, a torsional transient analysis of the drill string is performed to provide grounds for deciding the optimal way to mitigate or eliminate the stick-slip phenomenon.

2 THE NUMERICAL MODELS

2.1 Full scale model

The dynamic model consists of two degrees of freedom (DOF's) where the Surface Torque (STOR) is imposed at the top end. The dynamic characteristics of the top drive motor are not considered and the axial and lateral dynamics of the drilling system are neglected. Herein, the Bottom Hole Assembly (K_{BHA}) is assumed to be a rigid body since its stiffness is much greater than the stiffness of the drill pipe (K_{DP}), reaching two orders of magnitude, $Ratio = \frac{K_{DP}}{K_{BHA}} = 0,008$.

The full scale two DOF modelling is governed by Eq. 1, as follows. For convenience, the equations of motions are written as state-space (Eq.6).

$$\begin{bmatrix} J_1 & 0 \\ 0 & J_2 \end{bmatrix} \begin{bmatrix} \dot{\Omega}_1 \\ \dot{\Omega}_2 \end{bmatrix} + \begin{bmatrix} C_1 & -C_s \\ -C_s & C_2 \end{bmatrix} \begin{bmatrix} \Omega_1 \\ \Omega_2 \end{bmatrix} + \begin{bmatrix} k & -k \\ -k & k \end{bmatrix} \begin{bmatrix} \varphi_1 \\ \varphi_2 \end{bmatrix} = \begin{bmatrix} -T_1 \\ T_2 \end{bmatrix} \quad (1)$$

where T_1 is the Torque on Bit, T_2 is the STOR. J_1 and J_2 the equivalent moment of inertia at bottom end and top end, respectively. C_1 and C_2 are the mud damping, Ω_1 the bit speed and Ω_2 the top drive speed (Surface RPM - SRPM), C_s the structural damping, φ_1 and φ_2 the rotational displacement (angle) of the bit starting and top drive, respectively, with zero at time $t = 0$, and k is the equivalent stiffness of the drill pipe. Defining the lengths L_{DP} , L_{BHA} , the densities ρ_{DP} , ρ_{BHA} (kg/m^3), the outer diameters OD_{DP} , OD_{BHA} , the inner diameters ID_{DP} , ID_{BHA} , the area moments of inertia I_{DP} , I_{BHA} for the drill pipe, and the bottom hole assembly, respectively. We may write the equivalent mass moment of inertia

$$J_1 = \rho_{BHA} I_{BHA} L_{BHA}. \quad (2)$$

The area moments of inertia are given by

$$\begin{aligned} I_{BHA} &= \frac{\pi}{32} (OD_{BHA}^4 - ID_{BHA}^4), \\ I_{DP} &= \frac{\pi}{32} (OD_{DP}^4 - ID_{DP}^4). \end{aligned} \quad (3)$$

The stiffness is given by

$$k = \frac{G I_{DP}}{L_{DP}}. \quad (4)$$

where G is the shear modulus $G = \frac{E}{2(1+\nu)}$.

The mud damping is written in terms of a damping factor of the mud Dr ,

$$C_1 = Dr L_{DP}. \quad (5)$$

The structural damping is given by $C_s = 2\xi \sqrt{k} J_1$, where ξ is the damping factor. The matrices will be underlined.

$$\mathbf{q}' = \underline{\mathbf{A}} \mathbf{q} + \mathbf{T} \quad (6)$$

where $\underline{\mathbf{A}}$ is the matrix that contains the proprieties of the system, \mathbf{T} is the vector with efforts and \mathbf{q} is the state-space coordinate. Eq. 7 describes each member of Eq. 6, as following,

$$\mathbf{q} = \begin{bmatrix} \varphi_1 \\ \varphi_2 \\ \Omega_1 \\ \Omega_2 \end{bmatrix}, \underline{\mathbf{A}} = \begin{bmatrix} \mathbf{0} & \mathbf{I} \\ \underline{\mathbf{J}}^{-1}(-\underline{\mathbf{K}}) & \underline{\mathbf{J}}^{-1}(-\underline{\mathbf{C}}) \end{bmatrix}, \mathbf{T} = \underline{\mathbf{J}}^{-1} \begin{bmatrix} -T_1 \\ T_2 \end{bmatrix}. \quad (7)$$

The $\underline{\mathbf{I}}$ and $\underline{\mathbf{0}}$ denote the identity matrix and zeros matrix (2 x 2), respectively.

In 1994, Pavone and Desplans [6] developed a friction model from field data of the so-called Télévigile measurement device. The Télévigile was placed just above the bit and its function

is to measure and to transmit data about BHA dynamics [6]. Due the experimental origin of this model, Pavone's friction model is chosen as the friction model of the TOB in this work and is implemented using "look-up table" function (*Simulink*). Figure 2 illustrates the discussed friction model.

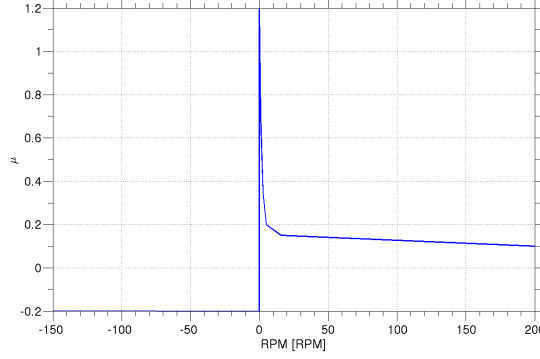


Figure 2: Pavone friction model.

2.2 Test rig model

The numerical test rig model consists of two DOF's - rotor 1 and the inertia of the DC-motor. The equations of the DC-motor are included into modelling. The axial and lateral motions are constrained by the bearings, and the structural damping is neglected.

The two DOF's modelling is governed by Eq. 8, as follows. The equations of the DC-motor are represented in Eq. 9 and, the equations of motions (mechanical and electrical) are written as state-space (Eq.10), as below:

$$\begin{bmatrix} J_1 & 0 \\ 0 & J_m \end{bmatrix} \begin{bmatrix} \dot{\Omega}_1 \\ \dot{\Omega}_2 \end{bmatrix} + \begin{bmatrix} 0 & 0 \\ 0 & C_m \end{bmatrix} \begin{bmatrix} \Omega_1 \\ \Omega_2 \end{bmatrix} + \begin{bmatrix} k & -k \\ -k & k \end{bmatrix} \begin{bmatrix} \varphi_1 \\ \varphi_2 \end{bmatrix} = \begin{bmatrix} -T_1 \\ k_T i - T_f \end{bmatrix} \quad (8)$$

$$\begin{aligned} L i' + R i + k_e \Omega_2 &= V \\ J_m \dot{\Omega}_2 + C_m \Omega_2 - k_T i &= -\tau \end{aligned} \quad (9)$$

$$\mathbf{q}' = \underline{\mathbf{A}} \mathbf{q} + \mathbf{F} \quad (10)$$

where φ_1 and φ_2 are the angular displacements of the rotor 1 and the inertia motor (J_m), respectively. Ω_1 and Ω_2 are the angular velocities, and i is the armature current of the DC-motor. C_m and k_T are speed regulation and constant torque of the DC-motor, respectively. The imposed dry friction torque to dissipate system energy is called T_1 . In terms of state-space equations, $\underline{\mathbf{A}}$ is the matrix that contains the proprieties of the system (mechanical and electrical), \mathbf{F} is the vector with efforts and \mathbf{q} stands for state variables. Further, k_e corresponds to the voltage constant, R and L are the armature resistance and inductance, respectively. Eq. 11 describes the variables of the first order system, the matrix $\underline{\mathbf{A}}$ and the efforts vector \mathbf{F} , as following,

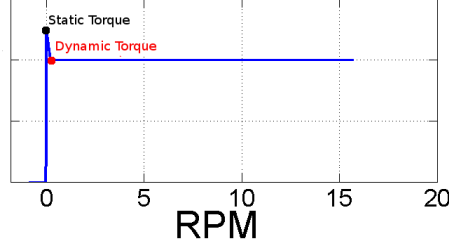


Figure 3: Applied modified Coulomb friction.

$$\mathbf{q} = \begin{bmatrix} \varphi_1 \\ \varphi_2 \\ \Omega_1 \\ \Omega_2 \\ i \end{bmatrix}, \quad \underline{\mathbf{A}} = \begin{bmatrix} 0 & 0 & 1 & 0 & 0 \\ 0 & 0 & 0 & 1 & 0 \\ -\underline{\mathbf{J}}^{-1}\underline{\mathbf{K}} & -\underline{\mathbf{J}}^{-1}\underline{\mathbf{C}} & 0 & 0 & 0 \\ 0 & 0 & 0 & -k_e/L & -R/L \end{bmatrix}, \quad \mathbf{F} = \begin{bmatrix} 0 \\ 0 \\ -T_1/J_1 \\ -T_f/J_m \\ V/L \end{bmatrix}. \quad (11)$$

As stated previously, the stick-slip is induced by dry friction imposed on rotor 1 (J_1) while J_m continues rotating with constant speed. Numerically, the friction torque T_1 consists of a modified Coulomb model, i.e., the model presents difference between the static and dynamic torque, T_{st} and T_{dyn} , respectively. If the velocity of rotor 1 is lower than a stipulated tolerance ($Tol = 0,001$) then the T_{st} is used, otherwise T_{dyn} is applied. The piecewise function of the T_1 is represented in Eq. 12 while Figure 3 illustrates the used friction model.

$$T_1 = \begin{cases} T_{st} & \text{if } \Omega_1 \geq Tol \\ T_{dyn} & \text{if } \Omega_1 < Tol \end{cases} \quad (12)$$

3 THE TEST RIG DESCRIPTION

The test rig consists of a DC-motor, one rotor (at the extremity position - rotor 1), a low-stiffness string is selected and a brake device is developed. Figure 4(a) illustrates the set-up of the test rig (the illustrated second rotor is not attached). The DC-motor is connected to the low-stiffness string which is responsible for transmitting rotational motion to the rotor. This rotor rotate around their geometric center and the lateral motions are constrained by bearings (neglected). The structural damping from the material is negligible.

The dry friction is imposed by a brake device at rotor 1 from a contact material in order to induce torsional vibrations. Figure [4(b) and Figure 4(c)] show the device which imposes a contact force on the radial end of the brake disc creating a resistive torque to the rotary motion. The device is composed by the brake pads and disc of a bicycle. The brake disc is acceded to the rotor 1, which means that rotor 1 and the disc keep the same angular speed over time. The brake pads are responsible for the contact with the brake disc, inducing dry friction.

In order to measure the speed at rotor 1 and at the DC-motor, rotary encoders *LS Mecapion* (1000 ticks/revolution) are used. The friction torque on rotor 1 is measured by a force sensor SV50 R-5 (*Alpha Instrumentos*) that it is mounted below the braking device (see Figure 4(c)) so that the friction torque is measured by a reaction force. The used acquisition board is the NI USB-6229 of *National Instruments*, and the applied DC-motor torque is measured by a force sensor of the PCB 208C01.

The actuation for opening and closing the pads is driven by an analogue servo controller *Dual-BB CS-80 Giant Scale* from the *HOBBICO Command Servos*.

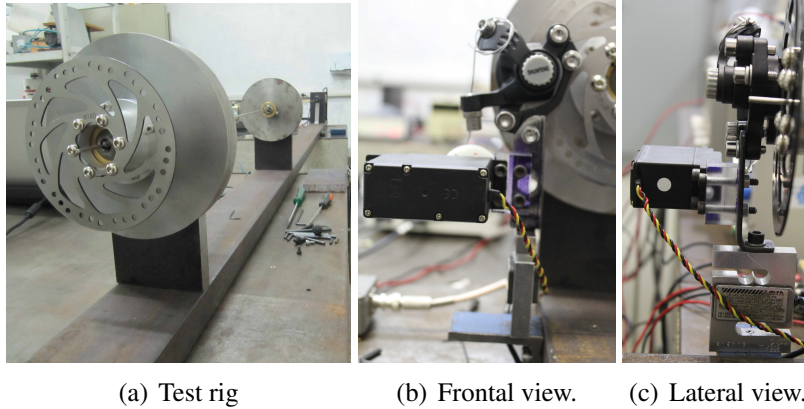


Figure 4: Test rig and brake device with force sensor.

4 RESULTS ANALYSIS

4.1 Numerical full scale results

Table 1 presents the used parameter values. The Bifurcation Diagram is conceived for each constant weight on bit (WOB). Also, the Bifurcation Diagram as a function of WOB is evaluated. In order to construct such diagram, the maximum and minimum angular velocity of the bit is computed.

Parameter	Description	Value	Unit
ρ_{dp}	Drill string mass density	7850	kg/m^3
L_{dp}	Drill string length	2780	m
OD_{dp}	Drill string outer diameter	139,7	mm
ID_{dp}	Drill string inner diameter	118,6	mm
ρ_{bha}	BHA mass density	7850	kg/m^3
L_{bha}	BHA length	400	m
OD_{bha}	BHA outer diameter	209,5	mm
ID_{bha}	BHA inner diameter	71,4	mm
E	Young's modulus	210	GPa
ν	Poisson ratio	0,3	—

Table 1: Numerical values of the drill string system.

As expected, the vibration range of SRPM increases when the WOB value is increased. Also, it is possible to observe the amplitude of vibration increasing with WOB (Figures 5(a) and 5(b)).

The vibration amplitudes when the WOB increases while the SRPM stays constant is evaluated. The vibration amplitudes increase when the WOB is increased, as expected (Figures 5(c) and 5(d)). The WOB effect on the bifurcation diagram is more visible.

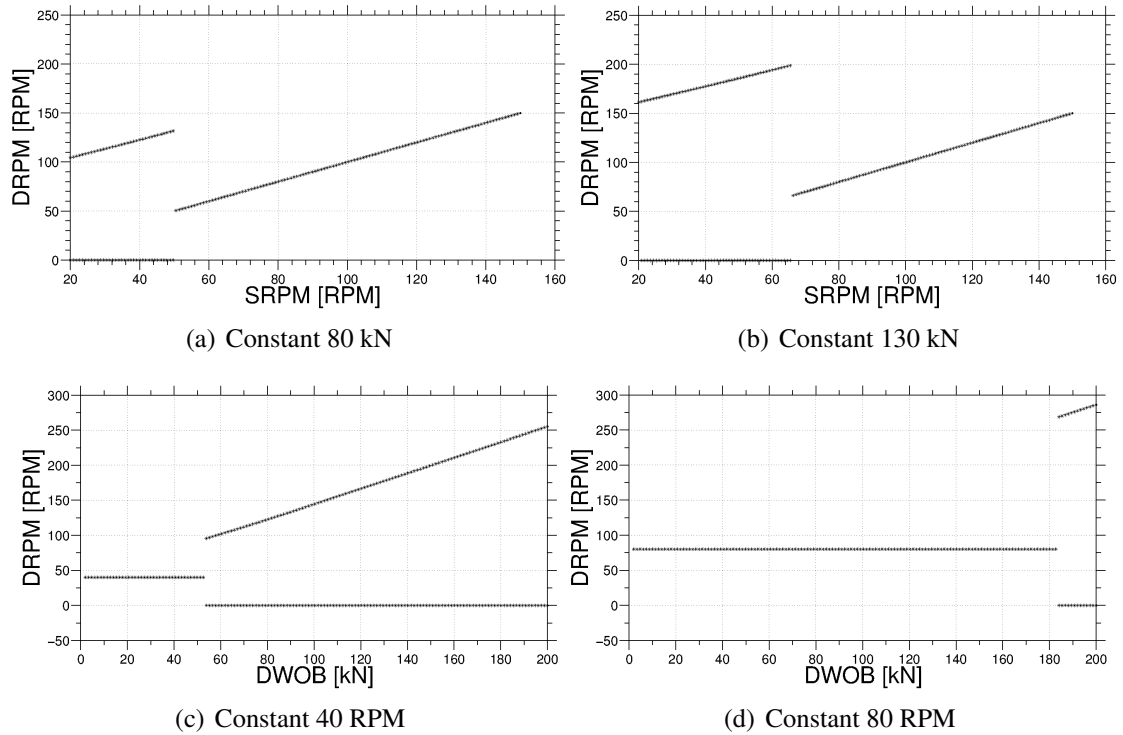


Figure 5: Bifurcation diagram with a constant WOB and RPM.

This behavior illustrates a bifurcation between an attractor of one dimension (limit cycle) and an attractor of zero dimension (fixed point), Figures 5(a) and 5(b), and vice-versa, Figures 5(c) and 5(d), representing an asymptotic behaviour [12]. In Figures 6(a) and 6(b) there is depicted the stable limit cycle of zero and one dimension, respectively.

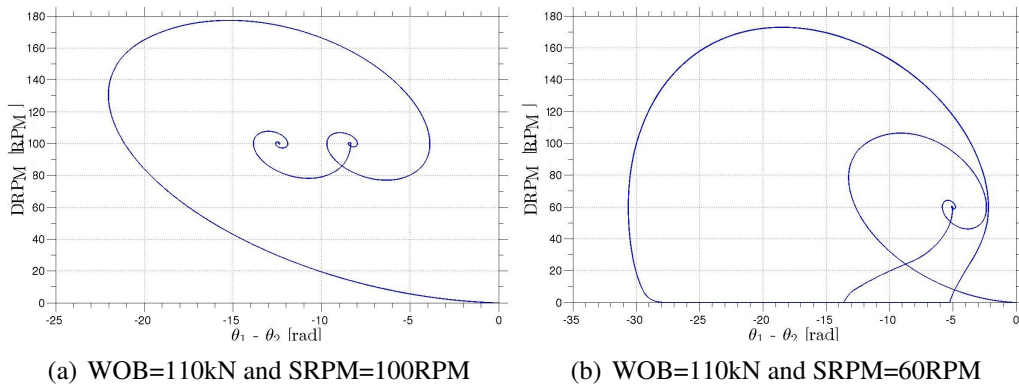


Figure 6: Limit cycle of zero and one dimension with initial conditions of 0 rad and 0 rad/s.

4.2 Experimental results of test rig

The first experimental task was to identify all the dynamic characteristics of the rig and define the scaling of the quantities to be measured. The rig shows to be reliable and adequate for its purpose. But the first results of testing the stick-slip conditions are being obtained at this exact moment and will be presented at the conference.

5 CONCLUSIONS

The approach of a full scale torsional drill string model aims to identify vibration zones, understanding phenomena and propose mitigation/elimination torsional vibrations. This work intends to explore this subject using the experimental validation of numerical models. It started with a rough description of the main phenomena at a real drill string, using parameter sensitivity analysis to find out the richness of results. In parallel a test rig was built and is being validated to reproduce characteristic dynamic behaviour of the real system. In a second step the rig will be used to optimize operation conditions.

Numerical results have shown that the torsional system does not present instability in its non-linear behaviour. There is a jump phenomenon, characteristic of non-linear systems, when the drilling condition jumps from a vibration zone to some no vibration zone, or vice-versa, depending of the [RPM x WOB] pair.

REFERENCES

- [1] F. Deily, D. Dareing, G. Paff, J. Orloff and R. Lynn, Downhole measurements of drill string forces and motions *Journal of Engineering for Industry*, **90**, 217–226, 1968.
- [2] P. Jogi and W. Zoeller, The application of a new drilling model for evaluating formation and downhole drilling conditions. *In: spe petroleum computer Conference , SPE 24452*, Houston, Texas, 1992.
- [3] J. Jansen. Nonlinear Dynamics of Oilwell Drillstrings. PhD thesis, Delf University Press. Delf, Netherlands, 1993.
- [4] M. Mattos. Sistemas amortecidos com atrito seco. Master thesis, Universidade de Campinas. Campinas, Brazil, 1993.
- [5] S. Strogatz, *Nonlinear Dynamics and Chaos: with applications to physics, biology, chemistry, and engineering*. Perseus Books, Massachusetts, 1994.
- [6] D. Pavone and J. Deplans, Application of high sampling rate downhole measurements for analysis and cure of stick-slip in drilling. *SPE 69th Annual Technical Conference and Exhibition*, Los Angeles, USA, 1994.
- [7] J. Jansen, L. van den Steen and E. Zachariassen, Active damping of torsional drillstring vibrations with a hydraulic top drive. *In: european petroleum conference, SPE 28911*, London, England, 1995.
- [8] J. Jansen, L. van den Steen and E. Zachariassen, Active damping self-excited torsional vibrations in oil well drill strings. *SPE Drilling & Completion*, **179**, 647–668, 1995.
- [9] A. Yigit and A. Christoforou, Coupled torsional and bending vibrations of drillstrings subject to impact with friction. *Journal of Sound and Vibrations*, **215**, 167–181, 1998.
- [10] E. Robnett, J. Hood and G. Macpherson, Analysis of the stick-slip phenomenon using downhole drillstring rotation data. *1999 spe/iadc drilling conference SPE/IADC 52821*, Amsterdam, Holland, 1999.

- [11] P. Spanos, A. Chavallier, N. Politis and M. Payne, Oil and gas well drilling: A vibrations perspective. *The Stock and Vibrations Digest*, **35**, 85–103, 2003.
- [12] M. Savi, *Dinâmica Não-Linear e Caos*. e-papers, Rio de Janeiro, Brazil.
- [13] L. Franca. Self-Excited Percussive-Rotary Drilling in Hard Rocks. PhD thesis, Pontifícia Universidade Católica do Rio de Janeiro. Rio de Janeiro, Brazil, 2004.
- [14] N. Mihajlović, A. van Veggel, N. van de Wouw and H. Nijmeijer, Analysis of friction-induced limit cycling in an experimental drill-string. *Journal of Dynamic Systems, Measurements and Control*, **126**, 709–720, 2004.
- [15] Y. Khulief, F. Al-Sulaiman and S. Bashmal, Vibration of analysis of drillstrings with self-excited stick-slip oscillations. *Journal of Sound and Vibration*, **299**, 540–558, 2007.
- [16] T. Ritto. Numerical Analysis of the Nonlinear Dynamics of a Drill-string with Uncertainty Modeling. PhD thesis, Université Paris-Est. Paris, France, 2010.
- [17] E. López, Bit-sticking phenomena in a multidegree-of-freedom controlled drill strings. Technical Report. University of Manchester, 2010.